

Impact of magnetic field on conjugate mixed convection heat transfer in a lid-driven triangular enclosure with an inclined wavy wall and internal heat generation

Daud Hasan, Arman Habib Polash, Hamim Faisal, Ahmed Imtiaz Rais, Md. Jisan Mahmud*

Department of Mechanical Engineering, Hajee Mohammad Danesh Science and Technology University, Dinajpur 5200, Bangladesh

ARTICLE INFO

Keywords:

Conjugate heat transfer
Mixed convection
Triangular enclosure
Wavy wall
Internal heat generation
Magnetohydrodynamics

ABSTRACT

This study numerically investigates conjugate mixed convection heat transfer, magnetohydrodynamic effects, and internal heat generation within a lid-driven triangular wavy enclosure with a rotating solid cylinder at its center. The significance of this work is to provide insights into the complex interplay of heat transfer, fluid flow, and magnetic field effects in a geometrically challenging enclosure for thermal management systems. The inclined chamber edges are stationary and maintained at a constant cold temperature, while a constant elevated temperature is applied to the uniformly sliding bottom edge. A steady magnetic field is applied to the enclosure while the solid cylinder rotates in a clockwise manner. By varying the Reynolds (31.623–316.23), Richardson (0.1–10), Grashof (10^3 – 10^5), and Hartman number (0, 50, 100) along a given speed ratio of the spinning cylinder, parametric simulation is performed. Qualitative findings are illustrated with streamline and isotherm plots. On the other hand, the quantitative thermal performance and flow characteristics of the configuration are determined by means of the average Nusselt number, average drag coefficient, normalized Nusselt number, as well as average fluid temperature. This investigation shows that the use of a magnetic field provides better control over the temperature distribution, along with a decreasing trend in heat transmission due to the rise in Hartmann number. The optimal design of the controlling parameters can be ascertained using the available detailed data.

1. Introduction

Mixed convection is a fundamental thermo-fluid phenomenon that includes forced and natural convection inside a zone of concern, manifested by the concurrent action of fluid flow driven via shear from mechanical influence and buoyancy from a thermal gradient. Several disciplines of technology, including cooling electronic and microelectronic equipment, solar collectors, heat exchangers, nuclear reactors, food processing, and solidification, demand the extensive use of mixed convection (Ali et al., 2022). Furthermore, recent research (Selimefendigil and Öztop, 2017) has focused on the internal generation or absorption of heat, which is caused by electrical current-conducting fluids, endothermic and exothermic chemical processes at the system interface, nuclear reactors, and various heat-producing physical events. When electricity is passed through a salted water solution, it generates internal heat. Therefore, internal heat absorption or generation occurring internally within the boundaries of the system demands careful

consideration in assessing a thermo-fluid system's thermal efficacy.

Mixed convection heat transfer within a triangular enclosure has substantial engineering applications, including building roof design, solar collectors, and electronic devices (Chamkha et al., 2018). A moving boundary of the enclosure enhances heat transmission along with the fluid flow characteristics. Many researchers (Selimefendigil and Öztop, 2017; Chamkha et al., 2018; Sojoudi, 2018; Shahid et al., 2021; Uddin et al., 2015; Selimefendigil et al., 2016) explored the heat transport and fluid flow features of mixed convection within differentially heated lid-driven triangular-shaped cavities. Two distinct sorts of studies have been identified along with various enclosure shapes (e.g., right angle, isosceles, equilateral). The first type emphasized on triangular cavities which have horizontal wall(s) (bottom/top) moving at a consistent velocity, whereas the other type concentrated on an enclosure that was heated differentially and had a uniformly moving side wall. Chamkha et al. (2018) examined magnetohydrodynamic (MHD) mixed convection within a triangular chamber that has the left vertical wall traveling at uniform velocity for a variety of pertinent factors. A reduction in heat

* Corresponding author.

E-mail addresses: imtiaz.me@hstu.ac.bd (A.I. Rais), jisanmahmud.me@hstu.ac.bd (Md.J. Mahmud).

Nomenclature	
Roman Symbols	
A	Dimensionless area of the fluid domain
A_m	Amplitude
B_0	Magnetic Field Strength
C_d	Average Drag Coefficient
C_p	Specific Heat Capacity (J/kg-K)
d	Diameter of Cylinder (m)
g	Gravitational Acceleration (m/s ²)
Gr	Grashof Number
Ha	Hartmann Number
k	Thermal Conductivity (W/m-K)
L	Length of the Side of The enclosure (m)
Nu	Average Nusselt Number
p	Pressure (Pa)
P	Non-Dimensional Pressure
Pr	Prandtl Number
Q	Internal Heat Generation (W/m ³)
Re	Reynolds Number
Ri	Richardson Number
T	Temperature (K)
u, v	Velocity Components (m/s)
U, V	Dimensionless Velocity Components
u_o	Top Lid's Sliding Velocity (m/s)
u_p	Cylinder's circumferential velocity (m/s)
Greek Symbols	
ϵ	Error (%)
β	Thermal Expansion Coefficient (1/K)
λ	Oscillation number
Δ	Thermal Heat Generation Coefficient
Θ	Dimensionless Temperature
μ	Dynamic Viscosity of fluid (Pa.s)
ρ	Density of fluid (kg/m ³)
Ω	Cylinder Speed Ratio
ω	Cylinder's Rotational Speed (Rad/s)
Subscripts	
av	Average
c	Cold
h	Hot
nor	Normalized
f	Fluid
s	Solid
Abbreviation	
CCW	Counter Clockwise
CW	Clockwise
MHD	Magnetohydrodynamics

transmission was noted when forced convection became dominant. The reduction in heat transfer was also noticed by Selimefendigil and Öztop (2017) who introduced nanoparticles along with the base fluid for enhanced performance. In another work by Sojoudi (2018), different amplitudes and frequencies of thermal forcing were examined at the lid-driven wall. It was discovered that increasing frequency results in a higher maximum value for the stream function, indicating a greater magnitude of fluid circulation within the cavity. For a top wall-driven cavity, Shahid et al. (2021) looked into mixed convection under a variety of controlling conditions within an isosceles triangular cavity. For the naturally occurring convection-dominated flow, they noticed an improvement regarding the heat transmission rate. In their investigations into the effect of a magnetic field within the enclosure, both Uddin et al. (2015) as well as Selimefendigil et al. (2016), found that the inclusion of a magnetic field in the enclosure delayed the convective flow, hence lowering the rate of heat transmission.

The aforementioned studies were conducted on lid-driven enclosures without any objects inside. However, the results of additional studies (Soomro et al., 2020; Hussain et al., 2023; Younis et al., 2023; Hussain et al., 2024; Selimefendigil et al., 2019; Amine et al., 2021) revealed that heat transmission performance was greatly enhanced due to a fixed or spinning cylindrical object being present within the differentially heated cavity. After examining the effects of four heaters placed at each quadrant of the cylindrical walls of the cavity, Hussain et al. (2024) found an increase in fluid velocity along a particular corner. One of the outstanding investigations was carried out by Selimefendigil et al. (2019). Their analysis concentrated on the effect of two different rotational orientations and the circular cylinder's rotational speed. It was discovered that the cylinder's counterclockwise rotation increased the rate of heat transport. As the cylinder's rotational speed increased, they also observed improved flow circulation. The literature review (Amine et al., 2021) also indicated that better heat transfer within the enclosure was achieved by enlarging the cylinder.

Among the different ways of heat transfer enhancement employed in cavity flows, the wavy channel has been identified as an effective passive method (Nishimura et al., 1984). The creation of flow recirculation

zones complicates the dynamics of flow within a wavy channel, even with laminar flow. Therefore, when developing thermal systems with corrugated channels, a deep understanding of the transport dynamics is crucial. Several research studies (Chowdhury and Alim, 2023; Shekar-amiz et al., 2021; Ali et al., 2023; Azizul et al., 2023; Cherif, 2022) examined how lid-driven cavity flows were affected by wavy walls and discovered that the recirculation zones found in wavy passageways are essential for increasing heat transmission. Ali et al. (2023) investigated mixed convection within a bottom wavy enclosure and discovered that wavy walls improved thermal performance. Additionally, they discovered that a greater undulation number was connected to a lower rate of heat transfer, leading them to conclude that an undulation number of three is ideal for improving flow characteristics and heat transmission. Azizul et al. (2023) examined magnetohydrodynamic mixed convection within a side-wavy chamber and discovered that, within the natural convection-dominated zone, a moderate undulation number offered the optimum heat transmission. In a triangular cavity, Cherif (2022) discovered that reduced irreversibility and improved heat transfer can be achieved with a low undulation number on a wavy wall.

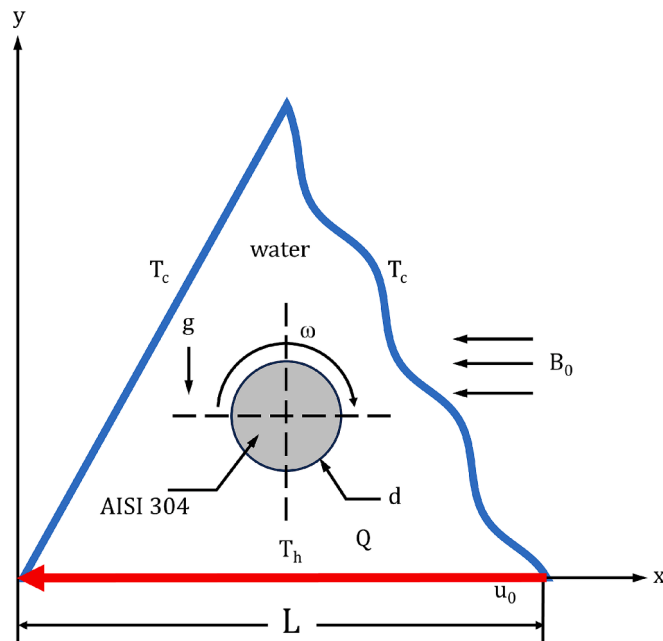
Magnetic field effects are crucial for numerous engineering application areas, including nuclear reactor coolers, molten metal purification, micro-electro-mechanical systems (MEMs), crystal growth processes, and energy storage process (Rahman et al., 2015; Oztop et al., 2011; Rahman et al., 2010; Ray and Chatterjee, 2014; Al-Salem et al., 2012). Convective heat transport may be regulated by an external magnetic field. During their excellent investigation of the magnetohydrodynamic effect, Rahman et al. (2010) discovered that the strength of the magnetic field has a noteworthy effect on the heat transmission properties as well as the fluid flow inside the enclosure, because a bigger Hartmann number decreases fluid circulation and lowers temperature gradients in the interior of the enclosure. The thermal and flow features regarding the mixed convective flow with MHD effect were thoroughly analyzed by Ray and Chatterjee (2014) and Al-Salem et al. (2012), who observed that the velocity field as well as the thermal fields could be efficiently governed by adjusting the applied magnetic field's strength.

The concurrent combination of heat transmission in both solids and

Table 1

Overview of published studies on conjugate mixed convection in various chambers with circular cylinder.

Author(s)	Sliding lid	Fluid (Pr)	Number of cylinder	Re	Ri	Gr	d/L	Ω
Chatterjee et al. (2014)	Left	Air (0.71)	1	100	0.1–10	10^3 – 10^5	0.2	-5,5
Paul et al. (2020)	Left	Air (0.71)	2	10–500	1	10 – 2.5×10^6	0.1–0.4	0.025,50
Chowdhury et al. (2021)	Right, Left	Air (0.71)	2	10–2000	1	10^2 – 4×10^6	0.2	-5,5
Mahmud et al. (2022)	Top	Water (5.85)	1	31.623–316.23	0.1–10	10^3 – 10^5	0.2	-0.1,0.1
Rasel et al. (2023)	None	Air (0.71)	2	31.623–316.23	0.1–10	10^4	0.2–0.4	-3,3
Islam et al. (2024)	None	Air (0.71)	1	32–316	0.1–10	10^3 – 10^5	0.2–0.4	None

**Fig. 1.** Schematics of the lid-driven triangular wavy chamber with a spinning solid cylinder.

fluids is known as conjugate heat transfer. While natural, forced, or mixed convection is common in fluids, conduction occurs in solid bodies. One way to modify the properties of heat transport in a cavity with mixed convection is to introduce an obstacle or heat-conducting object inside. The physical domain's forms, dimensions, and boundary conditions may greatly affect how well mixed-convection heat transfer works. Conjugate heat transmission within a variety of enclosure designs with a solid body that conducts heat—mostly mixed convection—was the subject of numerous research (Chatterjee et al., 2014; Paul et al., 2020; Chowdhury et al., 2021; Mahmud et al., 2022; Rasel et al., 2023; Islam et al., 2024; Tasnim et al., 2023; Jamy et al., 2023). Chatterjee et al. (2014) and Paul et al. (2020) investigated conjugate mixed convection with a rotating solid cylinder and found that the rotational speed of the solid cylinder has a considerable impact on the overall heat transmission. Furthermore, Mahmud et al. (2022) found the movement and formation of recirculation zones to be dependent on the direction of the rotating cylinder. Table 1 provides an overview of essential details on conjugate mixed convection that appeared in earlier studies regarding solid cylinder.

Internal heat generation-induced convection heat transmission has recently attracted much interest because of its many use cases in geophysics and energy-related engineering issues. Heat recovery from geothermal systems, especially big agricultural product storage systems, exothermic chemical reactions occurring within packed bed reactors, radiative cooling of molten glass, heating of flowing water within solar collectors, and nuclear fuel debris are examples of such applications (Chamkha, 2002). Chamkha (2002) discovered that the volumetric heat generation decreased the heat transmission for facilitating flow within a

differentially heated enclosure driven by the side lid. Many researchers (Sivasankaran et al., 2014; Saha, 2015; Mahmoudi et al., 2014; Selimfendigil and Öztürk, 2016; Abu Bakar et al., 2020; Hasan and Saha, 2024; Imtiaz Rais et al., 2023) concurred that the heat transmission phenomenon is significantly impacted by heat generation, regardless of the configuration of the cavity. Saha (2015) studied MHD mixed convection in a lid-driven cavity with internal heat generation/absorption and discovered that in a forced convection-dominated region, the effect of heat generation/absorption is not significant. One interesting piece of research was done by Imtiaz Rais et al. (2023), who investigated heat generation and absorption within an enclosure having a sliding top lid as well as a spinning solid cylinder inside. They found the impact of heat absorption to be significant for enhanced heat transmission along with consistent temperature distribution in the cavity.

A thorough examination of existing literature unveiled a notable absence of research investigating the combined impact of magnetic fields and internal heat generation on conjugate mixed convection within complex, enclosed systems. This study aims to bridge this knowledge gap by exploring the intricate interplay of these factors within a triangular enclosure. Introducing a rotating cylinder and differentially heated walls further complicates the thermal and fluid flow characteristics, necessitating a comprehensive analysis. By scrutinizing the influence of magnetic field strength on heat transfer attributes, this research seeks to contribute to the advancement of thermal management strategies in various engineering applications. The findings of this investigation have the possibility to influence the design and optimization of several engineering systems involving conjugate mixed convection heat transfer such as heat exchangers, solar collectors, chemical reactors, and exothermic chemical processes in rotating machinery. The findings of this study have direct implications for enhancing the thermal management of chemical reactors and solar collectors. By leveraging the insights gained from this investigation, engineers can optimize reactor design to improve efficiency and minimize heat losses. The understanding of fluid flow, heat transfer, and magnetic field interactions within the triangular enclosure provides valuable guidance for designing novel solar collector configurations that maximize energy capture.

2. Physical model

The physical characteristics of the triangular wavy enclosure under consideration within this study are depicted in Fig. 1. It includes an equilateral triangular wavy enclosure with sides L (in the cartesian coordinate system), as well as the appropriate boundary conditions. The enclosure's bottom lid is held at an elevated temperature $T_h (> T_c)$ and slides in a positive direction at a uniform speed of u_0 . The tilted side wall as well as the wavy wall of the enclosure maintains a fixed temperature of T_c . In the center of the chamber is a solid cylinder. The material of the cylinder is stainless steel (AISI 304) with a thermal conductivity of $k_s = 14.9$ W/mK. It rotates at a speed of ω in a clockwise direction. The cylinder's corresponding circumferential velocity is $u_p = \omega d/2$. Conversely, water with a Prandtl number of $Pr = 5.85$ along with a thermal conductivity of $k_f = 0.61$ W/mK acts as the working fluid inside the chamber. Gravity acts vertically and downward. Moreover, the system takes into account the internal heat generation rate related to the

working fluid, Q (W/m^3) along with a magnetic field of a given intensity, B_0 , which is uniformly applied in the negative x-direction.

3. Mathematical model

The governing equations for the current investigation are continuity of mass, conservation of momentum, as well as conservation of energy. Assuming a steady, two-dimensional, laminar flow in an enclosure comprising of a Newtonian and incompressible fluid that has constant thermo-physical properties, disregarding radiation and viscous dissipation, and utilizing the Boussinesq approximation for temperature-dependent density change, the current mathematical model can be represented as (Mahmud et al., 2022):

Fluid domain:

$$\frac{\partial u}{\partial x} + \frac{\partial v}{\partial y} = 0, \quad (1)$$

$$\rho \left(u \frac{\partial u}{\partial x} + v \frac{\partial u}{\partial y} \right) - \mu \left(\frac{\partial^2 u}{\partial x^2} + \frac{\partial^2 u}{\partial y^2} \right) + \frac{\partial p}{\partial x} = 0, \quad (2)$$

$$\rho \left(u \frac{\partial v}{\partial x} + v \frac{\partial v}{\partial y} \right) - \mu \left(\frac{\partial^2 v}{\partial x^2} + \frac{\partial^2 v}{\partial y^2} \right) + \frac{\partial p}{\partial y} - \rho g \beta (T - T_c) + \sigma B_0^2 v = 0, \quad (3)$$

$$\rho C_p \left(u \frac{\partial T}{\partial x} + v \frac{\partial T}{\partial y} \right) - k_f \left(\frac{\partial^2 T}{\partial x^2} + \frac{\partial^2 T}{\partial y^2} \right) - Q = 0, \quad (4)$$

Solid domain:

$$k_s \left(\frac{\partial^2 T}{\partial x^2} + \frac{\partial^2 T}{\partial y^2} \right)_s = 0, \quad (5)$$

The Cartesian coordinate system is defined by x and y , whereas the associated velocity components are u and v . Additionally, the quantities of T , p , B_0 , and g correspond to temperature, pressure, magnetic induction, and gravitational acceleration. Water has the following fluid properties: dynamic viscosity (μ), thermal expansion coefficient (β), specific heat at constant pressure (C_p), and density (ρ). Now, the nondimensional mathematical equations can be obtained by applying the scales as follows:

$$\text{Length: } X = \frac{x}{L}, Y = \frac{y}{L},$$

$$\text{Velocity: } U = \frac{u}{u_0}, V = \frac{v}{u_0},$$

$$\text{Temperature: } \Theta = \frac{T - T_c}{T_h - T_c}, \quad (6)$$

$$\text{Pressure: } P = \frac{p}{\rho u_0^2},$$

$$\text{Thermal heat generation coefficient: } \Delta = \frac{QL^2}{k_f(T_h - T_c)},$$

Incorporating the above dimensionless scales into governing equations produces the dimensionless equations as follows:

Fluid domain:

$$\frac{\partial U}{\partial X} + \frac{\partial V}{\partial Y} = 0, \quad (7)$$

$$U \frac{\partial U}{\partial X} + V \frac{\partial U}{\partial Y} - \frac{1}{Re} \left(\frac{\partial^2 U}{\partial X^2} + \frac{\partial^2 U}{\partial Y^2} \right) + \frac{\partial P}{\partial X} = 0, \quad (8)$$

$$U \frac{\partial V}{\partial X} + V \frac{\partial V}{\partial Y} - \frac{1}{Re} \left(\frac{\partial^2 V}{\partial X^2} + \frac{\partial^2 V}{\partial Y^2} \right) + \frac{\partial P}{\partial Y} - Ri\Theta + \frac{Ha^2}{Re} V = 0, \quad (9)$$

$$U \frac{\partial \Theta}{\partial X} + V \frac{\partial \Theta}{\partial Y} - \frac{1}{RePr} \left(\frac{\partial^2 \Theta}{\partial X^2} + \frac{\partial^2 \Theta}{\partial Y^2} \right) - \frac{\Delta}{RePr} = 0, \quad (10)$$

Solid domain:

$$K \left(\frac{\partial^2 \Theta}{\partial X^2} + \frac{\partial^2 \Theta}{\partial Y^2} \right)_s = 0, \quad (11)$$

Here, $K = k_s/k_f$ is the solid cylinder's to the working fluid's thermal conductivity ratio. Moreover, the additional nondimensional governing parameters are Reynolds number (Re), Hartmann number (Ha), Grashof number (Gr), Prandtl number (Pr), and Richardson number (Ri). The corresponding parameters' definitions are as follows:

$$Re = \frac{\rho u_0 L}{\mu}, Ha^2 = \frac{\sigma B_0^2 L^2}{\mu}, Gr = \frac{\rho^2 g \beta (T_h - T_c) L^3}{\mu^2}, Pr = \frac{\mu C_p}{k_f}, Ri = \frac{Gr}{Re^2}, \quad (12)$$

The interface conditions along with the non-dimensional boundary criteria regarding this study are displayed in Table 2, where X_c and Y_c are non-dimensional coordinates of the middle of the cylinder and Re_c is the rotational Reynolds number, depending on the circumferential velocity and diameter of the circular cylinder. Re_c is determined as follows (Mahmud et al., 2022);

$$Re_c = \frac{\rho u_0 d}{\mu} = \frac{\rho \omega d^2}{2\mu} \quad (13)$$

The description of the boundary and interface criteria of the system is as follows:

Bottom edge:

$$U = 1, V = 0, \Theta = 1 \text{ at } Y = 0 \text{ and } 0 \leq X \leq 1 \quad (14)$$

Left inclined edge:

$$U = 0, V = 0, \Theta = 0 \text{ at } Y = \sqrt{3}X \text{ and } 0 \leq X \leq 0.5 \quad (15)$$

Right wavy edge:

$$U = 0, V = 0, \Theta = 0 \text{ at } Y = -\sqrt{3}(X - 1) - 2A_m \left[1 - \cos \left\{ \pi \lambda (X - Y\sqrt{3} - 1) \right\} \right] \text{ and } 0.5 \leq X \leq 1 \quad (16)$$

For cylinder:

$$U = 2(Y - Y_c)(Re_c/Re)/(d/L), V = 2(X - X_c)(Re_c/Re)/(d/L), \Theta = K(\partial \Theta / \partial N)_s = (\partial \Theta / \partial N)_f \text{ at } (X - X_c)^2 + (Y - Y_c)^2 = (d/2L)^2 \quad (17)$$

The following definitions can be given to the average Nusselt number (Nu) related to the heated wall, the average fluid temperature (Θ_{av}) within the chamber, the average drag coefficient (C_d) of the sliding lid along with the normalized Nusselt number (Nu_{nor}) (Mahmud et al., 2022):

$$Nu = - \int_0^1 \frac{\partial \Theta}{\partial Y} \Big|_{Y=0} dX, Nu_{nor} = \frac{Nu(Ha \neq 0)}{Nu(Ha = 0)}, \\ C_d = \frac{2}{Re} \int_0^1 \frac{\partial U}{\partial Y} \Big|_{Y=1} dX, \Theta_{av} = \frac{1}{A} \int_A \Theta_f dA, \quad (18)$$

The subscripts "s" and "f," respectively, stand for the solid as well as fluid domains and the non-dimensional region of the fluid zone within the triangular chamber is represented by A . Additionally, for the right-inclined wavy wall, we have the dimensionless boundary condition as $A_m(1 - \cos(2\pi\lambda x))$. Here, A_m is the amplitude and λ is the oscillation number.

4. Numerical procedure

In the current research, the Galerkin finite element scheme is used to solve non-dimensional mathematical equations (7)–(11) as well as the appropriate boundary conditions mentioned in Table 2. The Galerkin finite element scheme excels in accurately approximating solutions to partial differential equations over complex domains. This method entails discretizing the computing area into a finite number of irregular triangular or rectangular cells. According to this method, triangular

Table 2

Boundary and interface criteria of the system utilized in the investigation.

Parameters	Bottom	Left inclined	Right inclined wavy	Solid Cylinder Surface
U	1	0	0	$2(Y - Y_c)(Re_c/Re)/(d/L)$
V	0	0	0	$2(X - X_c)(Re_c/Re)/(d/L)$
Θ	1	0	0	$K(\partial\Theta/\partial N)_s = (\partial\Theta/\partial N)_f$

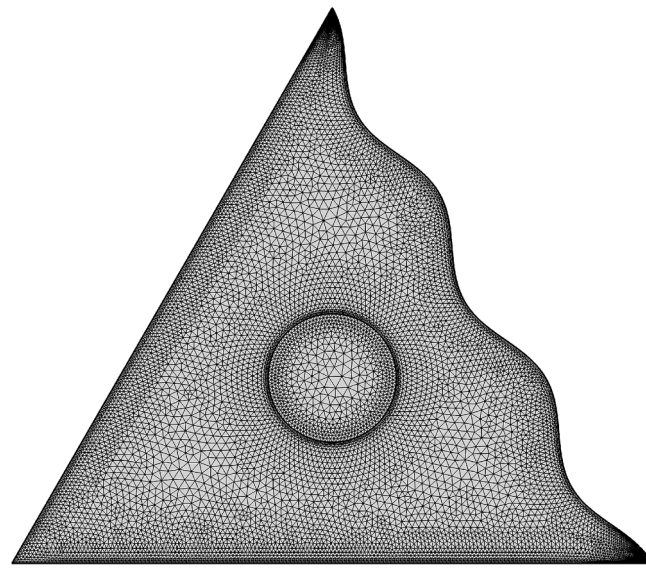


Fig. 2. Mesh distribution used in the study following grid refinement analysis.

elements are utilized for creating finite element equations. The mesh structures regarding the full domain equipped with triangular elements are depicted in Fig. 2. Afterward, The Galerkin weighted residual method is utilized to convert the nonlinear governing equations, which include mass, momentum, as well as energy conservation equations. The governing equations are converted to a set of integral equations. Then, the application of boundary conditions modifies the nonlinear algebraic equations that have been acquired. The modified nonlinear equations are converted into linear algebraic equations employing Newton's approach. Subsequently, the linear equations are resolved utilizing triangular factorization. A specific upper constraint is set for numerical solution error estimates and convergence. The solution technique is continued prior to the convergence conditions being met. The discretization approach used in this investigation results in fast convergence as well as reliable results.

4.1. Grid refinement analysis

For better accuracy and faster prediction times, a grid refinement analysis is executed prior to parametric simulation, which can be visualized in Fig. 3. The Nusselt number variation and accompanying error (ϵ) are depicted in this figure using the incremental element number. The following method is used to calculate the computational error in this analysis (Tasnim et al., 2023):

$$\epsilon = \left| \frac{Nu_c - Nu_i}{Nu_c} \right| \times 100\% \quad (19)$$

Nu_c and Nu_i represent the convergent Nusselt number and the individual Nusselt number, respectively, when discussing numerical simulation. In order to maximize processing efficiency and time, the mesh quality and density are considered with great care. Fluid flow, heat transmission, and all boundary conditions are taken into account while designing non-uniform and structured cells during meshing. There are finer meshes surrounding the sides of the chamber and the surfaces of the revolving circular cylinders. The distribution of heat and fluid

systems in the chamber is accurately portrayed in the generated grids. Grid refinement findings for $Re = 100$, $Re_c = -2$, $Gr = 10^5$, $K = 24.43$, $\Delta = 10$, $d/L = 0.2$, $Ha = 50$, and $Pr = 5.85$ are expressed as average Nusselt number are illustrated in Table 3. To identify the optimal mesh configuration for the model, a parametric sweep is employed, evaluating a range of element arrangements from highly coarse to highly refined. Lastly, a 22,804 element extra-fine mesh is chosen, and it has been proven that it is adequate because the average Nusselt number has not significantly changed. Table 4 provides comprehensive details of the "extra fine mesh" type that was chosen.

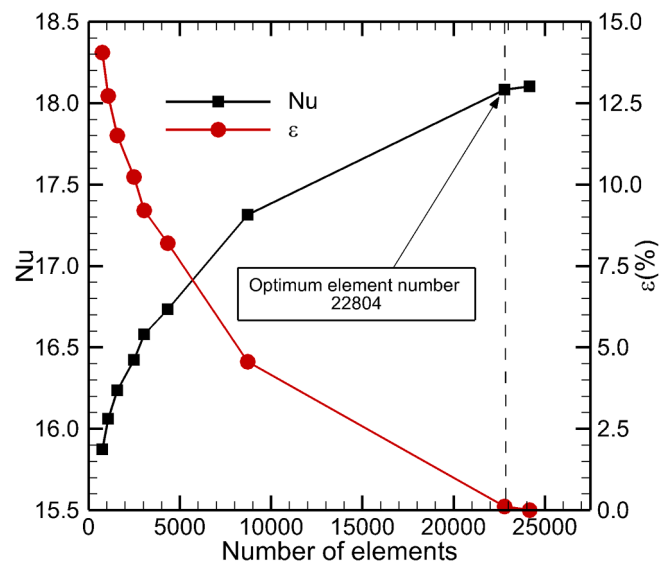


Fig. 3. Grid refinement check and the optimum element number for the current study.

Table 3

Grid refinement analysis.

Element Number	Node Number	Nu
766	578	15.8722
1067	775	16.0602
1583	1096	16.2352
2494	1649	16.4216
3051	1977	16.5789
4351	2732	16.7324
8719	5168	17.3134
22,804	12,813	18.0816
24,178	13,553	18.1029

Table 4

Comprehensive information about the optimal mesh type chosen (Extra fine).

Information about the Mesh	Statistics of the Mesh
Element quantity	
Triangles	20,852
Quads	1952
Vertex elements	9
Edge elements	976
Overall	22,804
Average elements quality	0.7892

4.2. Model validation

To verify the validity of any computational model and associated simulation tool, previously published research should be analyzed using the current simulation technique.

For that reason, the present model has been validated utilizing the outcomes of Mahmud et al. (2022) for the conjugate mixed convective flow of water in a square enclosure and the internal heat production effect. As part of the verification process, the average Nusselt number is computed in order to assess the computational model's accuracy and dependability. The current model is quantitatively verified for two different rotating directions in Fig. 4. The current model produces numerical results that are reasonably close to the data that has been published. The new model is additionally validated using the information provided by Rahman et al. (2010), which includes the magnetohydrodynamic term. From Fig. 5, it is evident by evaluating both outcomes that the agreement is satisfactory. This gives us the confidence to continue with the computations for various parameters.

5. Results and discussion

Following a proper grid refinement study and validation of the current model, the current problem's parametric simulation is executed while maintaining the subsequent physical as well as governing parameters fixed: $Pr = 5.85$, $A_m = 0.025$, $\lambda = 3$, $\Delta = 10$, $K = 24.43$, $Re_c = -2$, and the ratio of diameter to length (d/L) = 0.2. Table 5 presents a summary of the governing parameter ranges chosen for the parametric simulation, categorized into three groups of case studies. For every case, we determine the distribution of the Nusselt number of the heated bottom wall, the change of the normalized Nusselt number related to the magnetic effect, the change in drag coefficient associated with the sliding lid of the chamber, as well as the measurement of the average bulk water temperature within the chamber. Furthermore, streamlines along with isotherms are also shown systematically for qualitative illustration and an improved comprehension of fluid flow and heat transmission.

5.1. Effect of Ha and Gr at a fixed value of Re

Fig. 6 shows how the magnetic field intensity inside a lid-driven enclosure affects the overall thermal performance of the system under investigation for numerous Ri and Gr . Furthermore, the findings offer

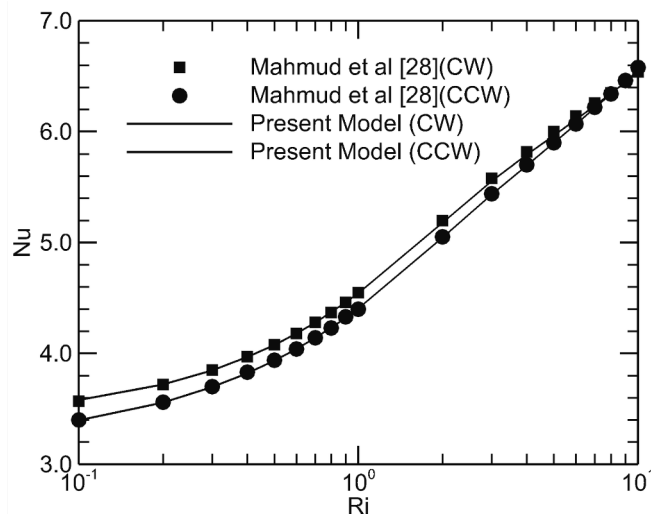


Fig. 4. Comparison of outcomes between the present model and Mahmud et al. (Mahmud et al., 2022) showing the variation of Nu with Ri for $Re = 100$, $K = 24.43$, $Re_c = \pm 2$, $\Delta = 10$, $Pr = 5.85$, $d/L = 0.2$.

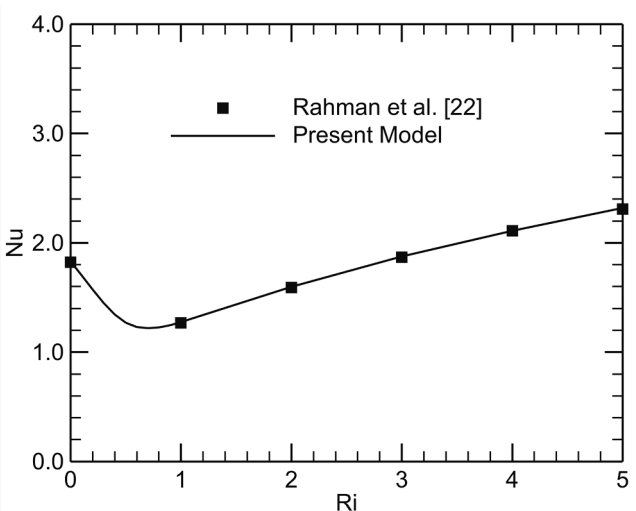


Fig. 5. Comparison of outcomes between the present model and Rahman et al. (Rahman et al., 2010) illustrating the variation of Nu with Ri for $Ha = 10$, $Re = 100$, $Pr = 0.71$.

Table 5

Overview of the present investigation's non-dimensional regulating parameters.

Case	Ri	Re	Gr	Ha
1	0.1–10	100	10^3 – 10^5	0,50,100
2	0.1–10	31.623–316.23	10^4	0,50,100
3	1	31.623–316.23	10^3 – 10^5	0,50,100

comparative information with a non-magnetic configuration in the enclosure. Fig. 6(a) illustrates a reduction in the average Nusselt number with a rise in the Hartmann number because the Lorentz force retards convection within the enclosure. However, between the range of Ri number, the change of Nu is insignificant when Ha is fixed. As the strength of the magnetic field rises, it suppresses convection more. Furthermore, the figure demonstrates that, in the existence of an increased magnetic effect, forced convection and free convection heat transfer are similar, but in the lack of a magnetic field in the chamber, the heat transmission differs significantly within the natural convection-dominated region. The enclosure's undulating wall also has an interesting influence on the overall heat transmission rate. When the effect of the magnetic field is absent, a reduced heat transmission at an elevated Richardson number is caused by flow separation and disturbance of smooth laminar flow at the wavy wall when the flow transitions to natural convection. As the magnetic field strength grows, the overall thermal distribution becomes more uniform due to the retardation by the Lorentz force which enhances mixing.

Fig. 6(b) indicates how the fluctuation of the Ri and Gr affects the normalized Nusselt number when the lid velocity remains fixed ($Re = 100$). Even though there exists a drop in the rate of heat transfer while the flow transitions from forced to natural convection, we notice a rise in heat transfer rate with an increase in Ri for $Ha = 50$ and $Ha = 100$.

Fig. 7(a) illustrates how the average drag coefficient varies with various values of Ri and Gr , for different magnetic effects at a fixed Re . For a fixed Ha , the average drag coefficient remains essentially unchanged with a variation of Ri and Gr . A slight increase can be noticed for the non-magnetic effect situation due to the formation of secondary vortices in the enclosure when the flow is at natural convection. Furthermore, with a rise in magnetic field strength, the magnitude of the average drag coefficient rises due to flow retardation by the magnetic field. Fig. 7(b) illustrates the change in average fluid temperature with various values of Ri and Gr . Since the temperature of the fluid achieves stronger thermal stratification as well as stabilization with a rising temperature gradient corresponding to higher Ri and Gr , it behaves

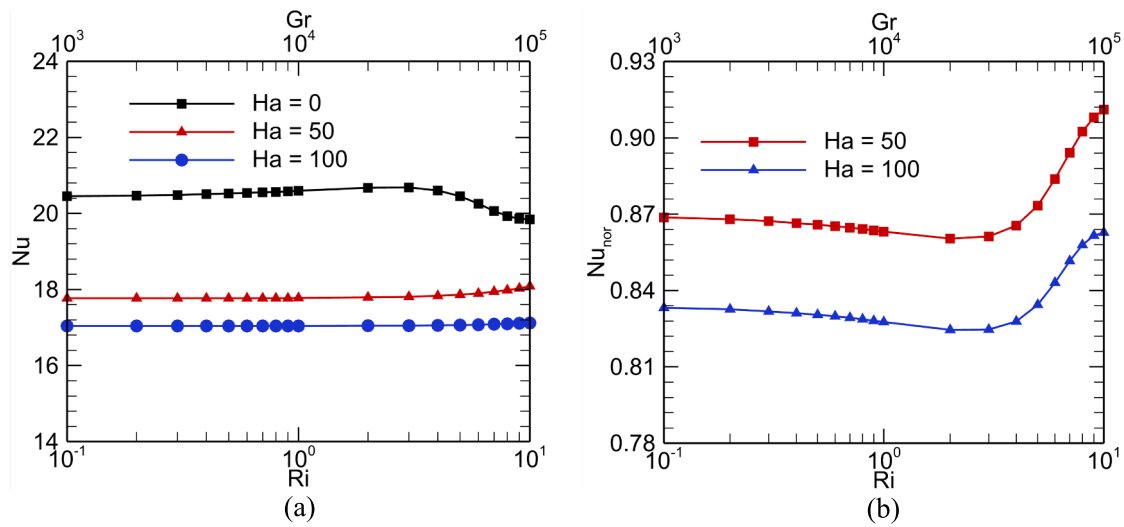


Fig. 6. Observation of (a) Nu and (b) Nu_{norm} for several values of Gr and Ri with an increase in Ha at $Re = 100$.

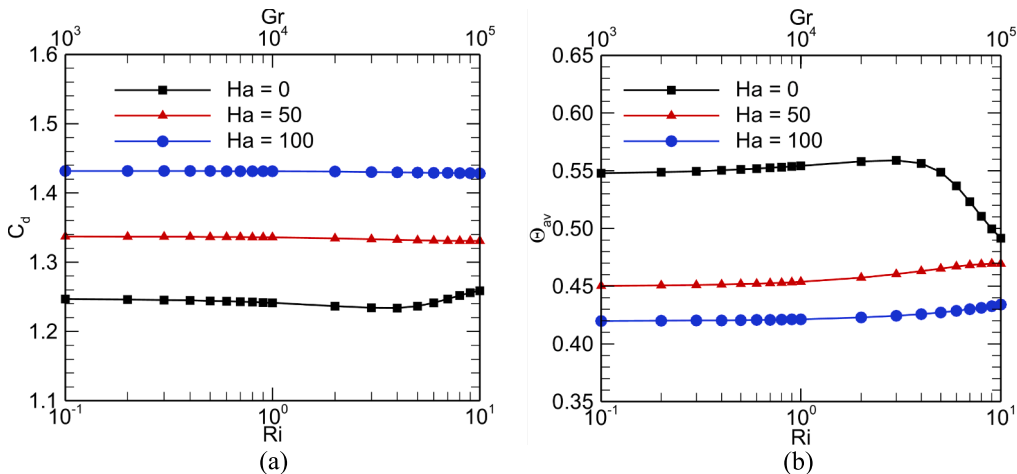


Fig. 7. Variations of (a) C_d and (b) θ_{av} with Ri and Gr for a range of Ha values at $Re = 100$.

similarly to the average Nusselt number associated with numerous Ha , as illustrated in Fig. 6(a).

The effect of the Gr and Ri regarding the streamlines of three distinct Hartmann number values at $Re = 100$ is depicted in Fig. 8(a)–(i). These figures demonstrate that the streamline pattern is significantly affected by the magnetic effect, particularly in situations with strong magnetic fields. Furthermore, without the magnetic effect, a secondary vortex is formed which revolves in the counter clockwise manner for the pure natural convection scenario. This secondary vortex opposes the primary vortex which revolves in the clockwise direction, eventually reducing the overall heat transmission inside the cavity. We see flow separation associated with a rise in the number of circulation zones inside the cavity as the Hartmann number increases, which would ensure effective fluid mixing within the cavity. This eventually results in a uniform temperature across the cavity, as seen in Fig. 8(b).

Fig. 9(a)–(i) shows how various Hartmann numbers affect isotherms for numerous Ri and Gr values when Re is maintained at 100. For a non-magnetic situation, the temperature distribution is uneven for different Ri and Gr values.

The effect of the wavy wall is also more pronounced as the lid velocity of the cavity decreases and flow becomes dominated by natural convection. Around $Ri = 10$, which represents the natural convection-dominated zone, stronger gradients in the isotherms are witnessed. As

the magnetic field intensity increases, the isotherms become more stable, even though flow transitions to different convection regimes. This guarantees a consistent temperature distribution within the cavity and can be used in real-world situations where exact control over the temperature distribution is required. As the wavy wall's effect becomes insignificant at larger Ha , it is possible to use the magnetic field effect to optimize and control the temperature inside complicated and unusual geometries.

5.2. Effect of Ha and Re at a fixed value of Gr

Fig. 10(a) illustrates the impact of magnetic field intensity upon the enclosure's average Nusselt number in addition to a variation of Re and Ri . In this case, Nu exhibits an inverse relationship with Ri at constant Gr , primarily due to the significant reduction in Re associated with the sliding lid velocity.

Heat transmission from the bottom wall progressively decreases when the lid velocity drops because the fluid velocity inside the enclosure reduces. In addition, magnetic field strength which effectively reduces the total heat transmission rate, is an important element in heat transmission. This is noticed in Fig. 10(b) as likewise noted in the previously stated case (see Fig. 6(b)).

Variation of average fluid temperature and average drag coefficient

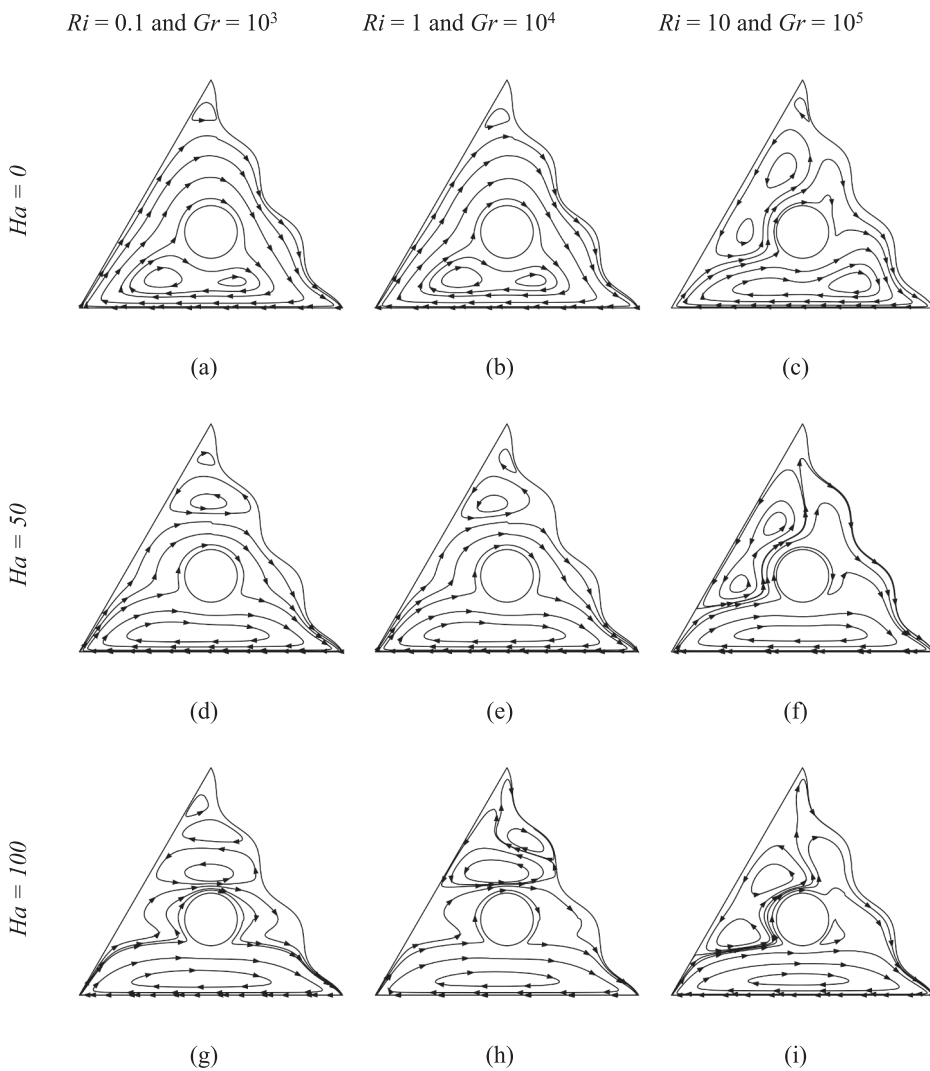


Fig. 8. Streamlines for various Ri and Gr at (a)–(c) $Ha = 0$, (d)–(f) $Ha = 50$, (g)–(i) $Ha = 100$ when Re is kept constant at 100.

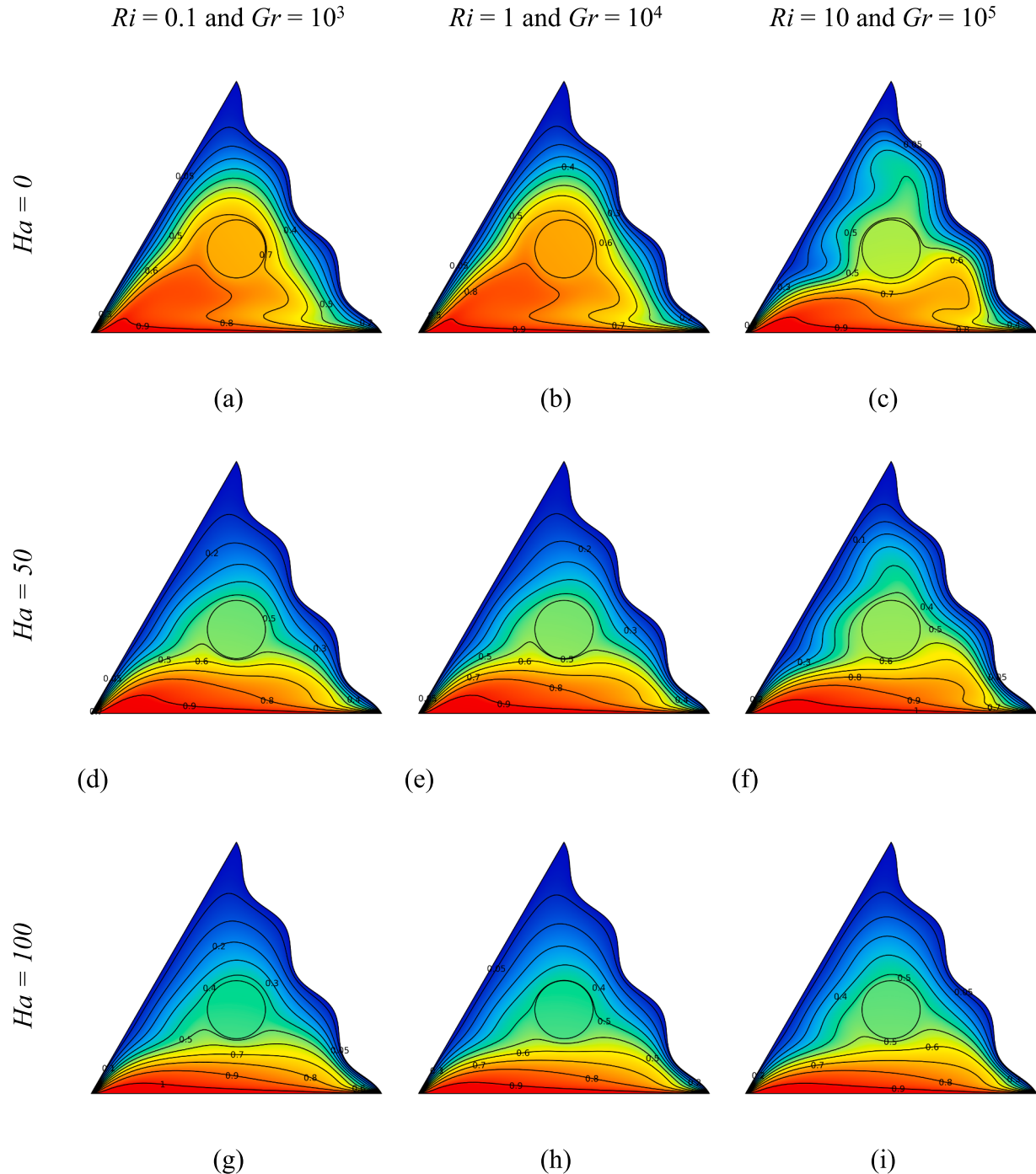


Fig. 9. Isotherms for various Ri and Gr at (a)–(c) $Ha = 0$, (d)–(f) $Ha = 50$, (g)–(i) $Ha = 100$ when Re is kept constant at 100.

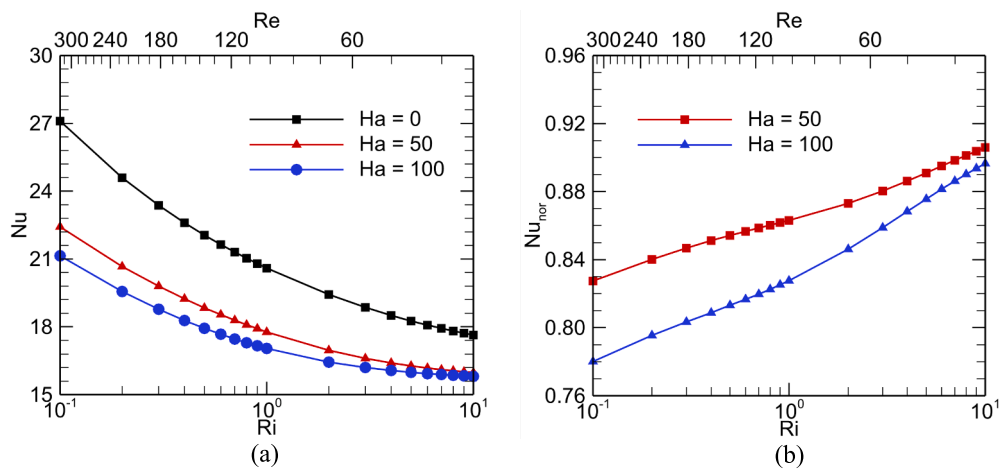


Fig. 10. Observation of (a) Nu and (b) Nu_{nor} for several values of Re and Ri with an increase in Ha at $Gr = 10^4$.

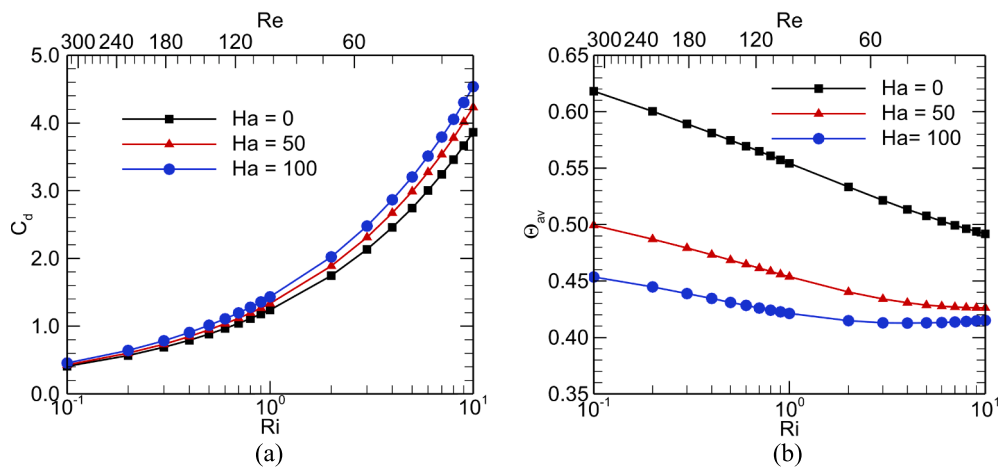


Fig. 11. Variations of (a) C_d and (b) θ_{av} with Re and Ri for a range of Ha values at $Gr = 10^4$.

with varying Ha with different Re and Ri are displayed in Fig. 11(a) and (b). Regardless of the value of Ha , the heated fluid at the bottom lid moves upward due to natural convection, which is more significant for a lower Reynolds number flow. This causes a sudden increase in the average drag coefficient due to the decrease in the overall fluid velocity along with a reduced Re number. For any scenario involving Ha , the average fluid temperature within the chamber drops; this impact is strongest in situations where there is a large magnetic effect. As the cavity's sliding lid is the heated wall, reduced Re results in a lower overall temperature in the cavity. Moreover, the magnetic field also diminishes the average temperature within the enclosure, which is consistent with earlier findings.

Streamline plots for numerous values of Ha , Ri , and Re are shown in Fig. 12(a)–(i), with Gr held constant. As the heat transmission moves from forced towards natural convection, vortex formation in the bottom side of the enclosure decreases dramatically and shifts towards the cylinder. This results from the sliding lid's decreased velocity in relation to the cylinder's velocity. A decrease in Re is accompanied by a reduction in lid velocity. This translates to a diminishing relative velocity

between the lid and the cylinder, consequently attenuating the secondary flow patterns along the cavity's bottom surface. This action is negated by the magnetic field effect, and we see several eddies emerging within the enclosure.

In Fig. 13(a)–(i), isotherm plots with varying Ha , Ri , and Re are displayed at a constant Gr . In the non-magnetic effect situation, isotherms shift considerably when the Reynolds number, or moving lid speed, changes. A higher Re value suggests a more widespread forced convection phenomenon, wherein the heated fluid flows over a broader region within the enclosure. The fluid which is heated at the bottom wall moves upward towards the inclined cool walls as the flow changes into a natural convection dominated zone. This causes a faster dissipation of heat and less heat accumulation inside the enclosure. Furthermore, the magnetic field effects ensure that the temperature inside the enclosure is distributed uniformly and also minimize hot spots in the forced convection regime.

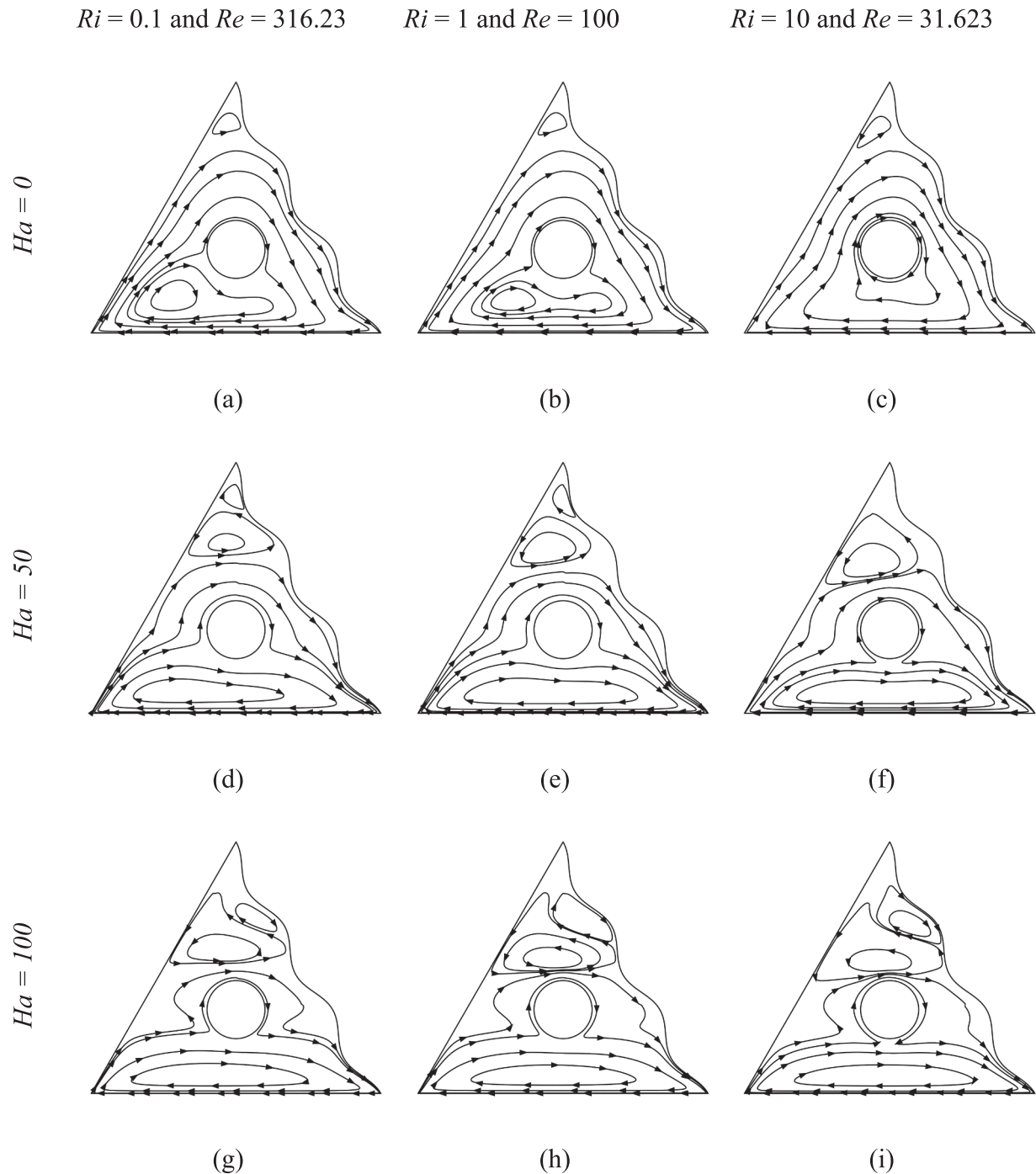


Fig. 12. Streamlines for various Ri and Re at (a)–(c) $Ha = 0$, (d)–(f) $Ha = 50$, (g)–(i) $Ha = 100$ when Gr is kept constant at 10^4 .

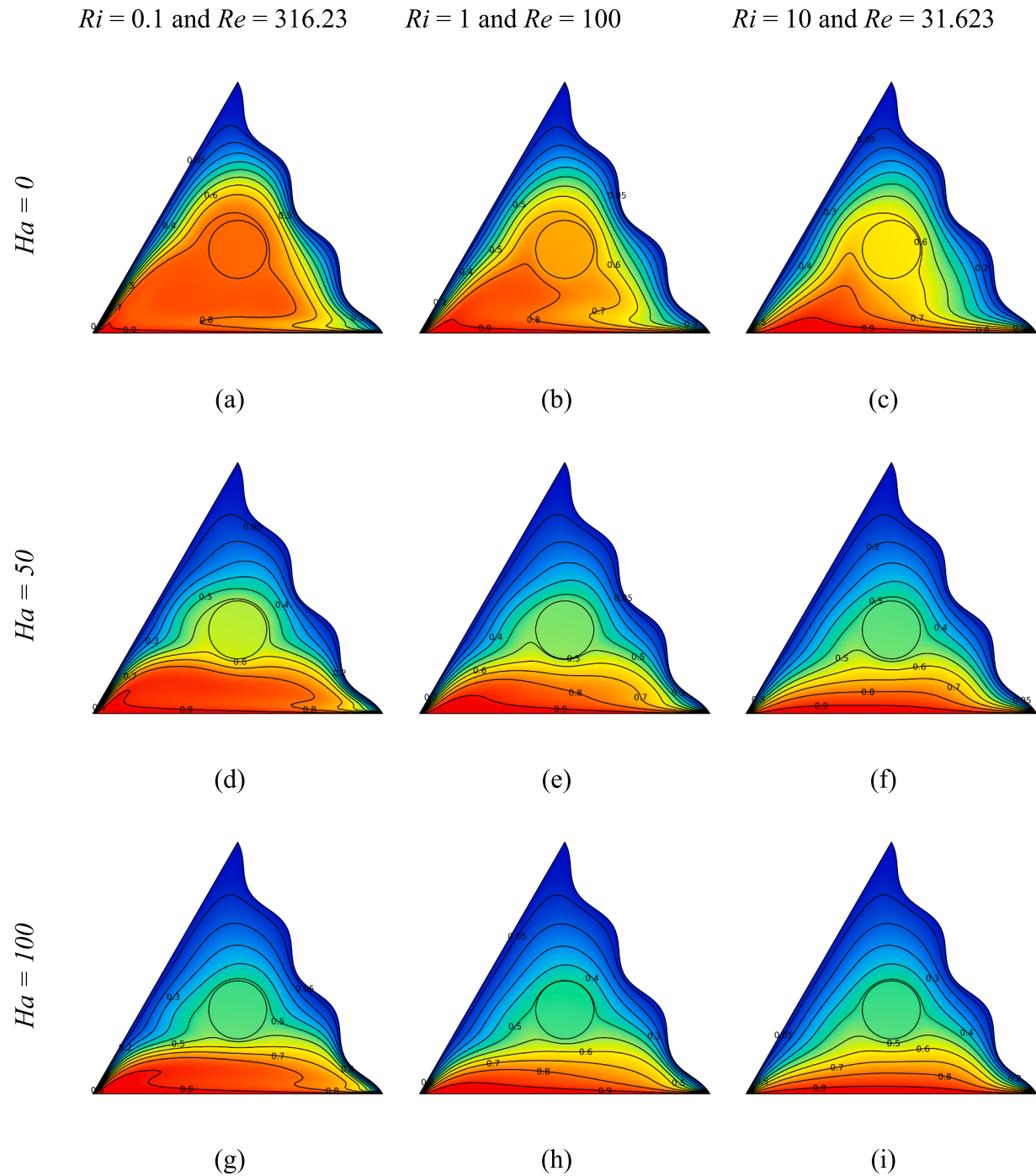


Fig. 13. Isotherms for various Ri and Re at (a)–(c) $Ha = 0$, (d)–(f) $Ha = 50$, (g)–(i) $Ha = 100$ when Gr is kept constant at 10^4 .

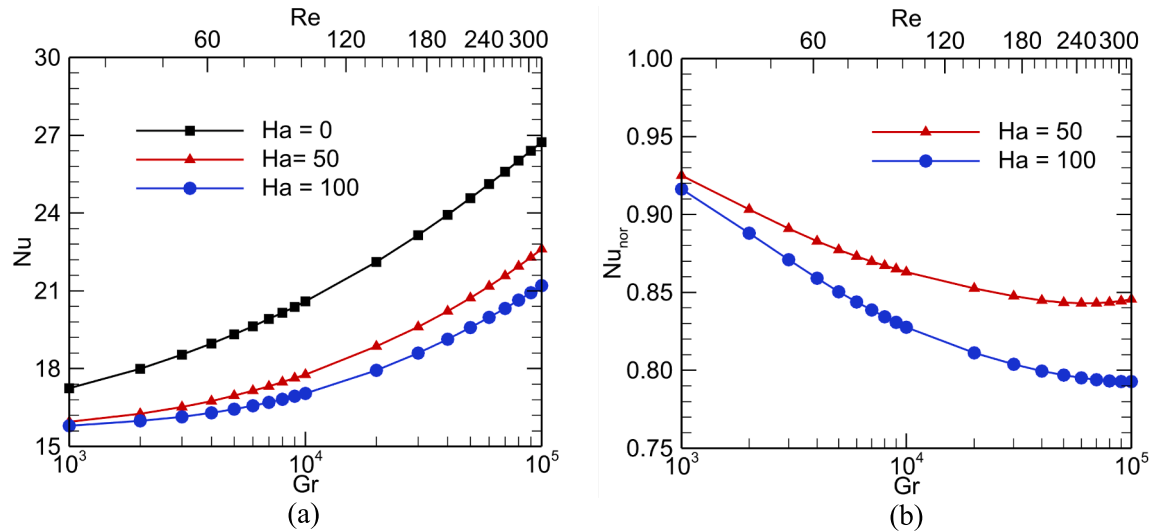


Fig. 14. Observation of (a) Nu and (b) Nu_{nor} for several values of Re and Gr with an increase in Ha at $Ri = 1$.

5.3. Effect of Ha , Gr and Re at a fixed value of Ri

To analyze the impact of all controlling parameters, the pure mixed convection scenario with a Richardson number of 1 is utilized, and both quantitative as well as qualitative assessments of the system's overall performance is carried out. Fig. 14(a) shows an upward trend in heat transmission along with a rise in Re and Gr . A higher lid velocity eventually draws more heat from the heated wall by forcing the fluid to circulate within the cavity. With a rise in Re as well as Gr , the lid velocity and temperature gradient increase, resulting in improved overall heat transmission. Additionally, there is a reduction in the magnitude of average Nu associated with a rise in Ha , which can be witnessed in Fig. 14(b).

Fig. 15(a) and (b) illustrate that increasing the parameters Re and Gr while maintaining fixed Ri , reduces the moving lid's average drag coefficient along with the fluid's average temperature. Either the viscous force will diminish or the buoyant force will rise with a rise in Gr . Thus, as Grashof number grows, the fluid inside the enclosure travels faster. However, for greater Re , the moving lid speed will rise, highlighting the

cold mixing fluid circulation inside the enclosure. The fluid's increased velocity also causes the process of cooling around the cylinder to accelerate and become more uniform.

The impacts of Ha and the simultaneous impact of Gr and Re on isotherm and streamline illustrations are shown in Figs. 16(a)–(i) and 17 (a)–(i), respectively. From Fig. 16, it can be inferred that when $Ri = 1$, as Re and Gr grow, there are more eddies on the upper portion of the enclosure and along the cylinder. The fluid is driven toward different areas of the enclosure by the top lid's greater velocity along with the enclosure's higher temperature gradient. A stronger magnetic field causes many more vortices to form; these are particularly noticeable in flows where free convection predominates. The rise in the velocity of the lid along with the thermal gradient throughout the enclosure's inclined walls and bottom wall causes the average fluid temperature to rise considerably because of the previously stated cause. Fig. 17 presents this evident truth. This effect decreases with a rise in magnetic field strength and the fluid temperature appears to be more consistent at the maximum Hartmann number.

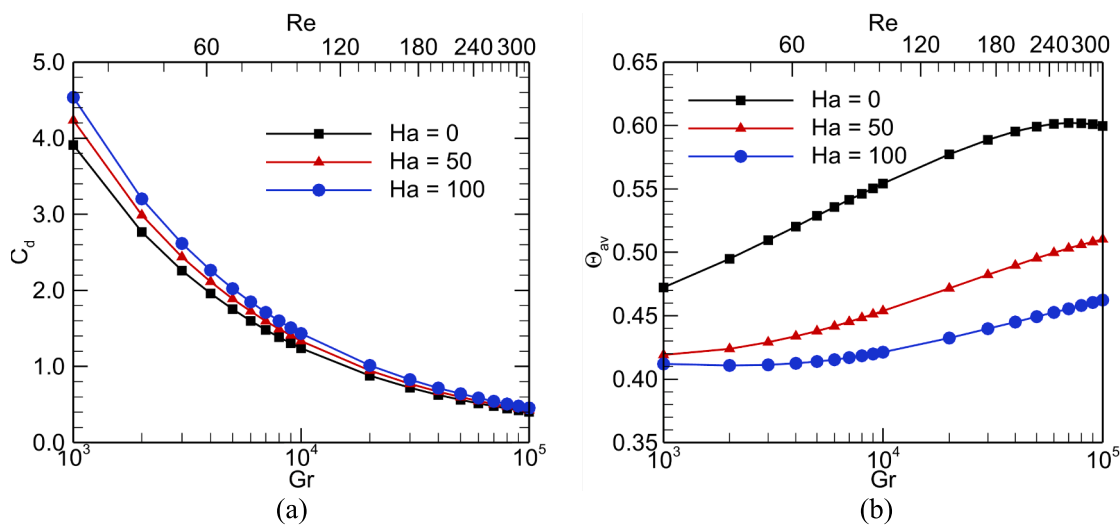


Fig. 15. Variations of (a) C_d and (b) θ_{av} with Gr and Re for a range of Ha values at $Ri = 1$.

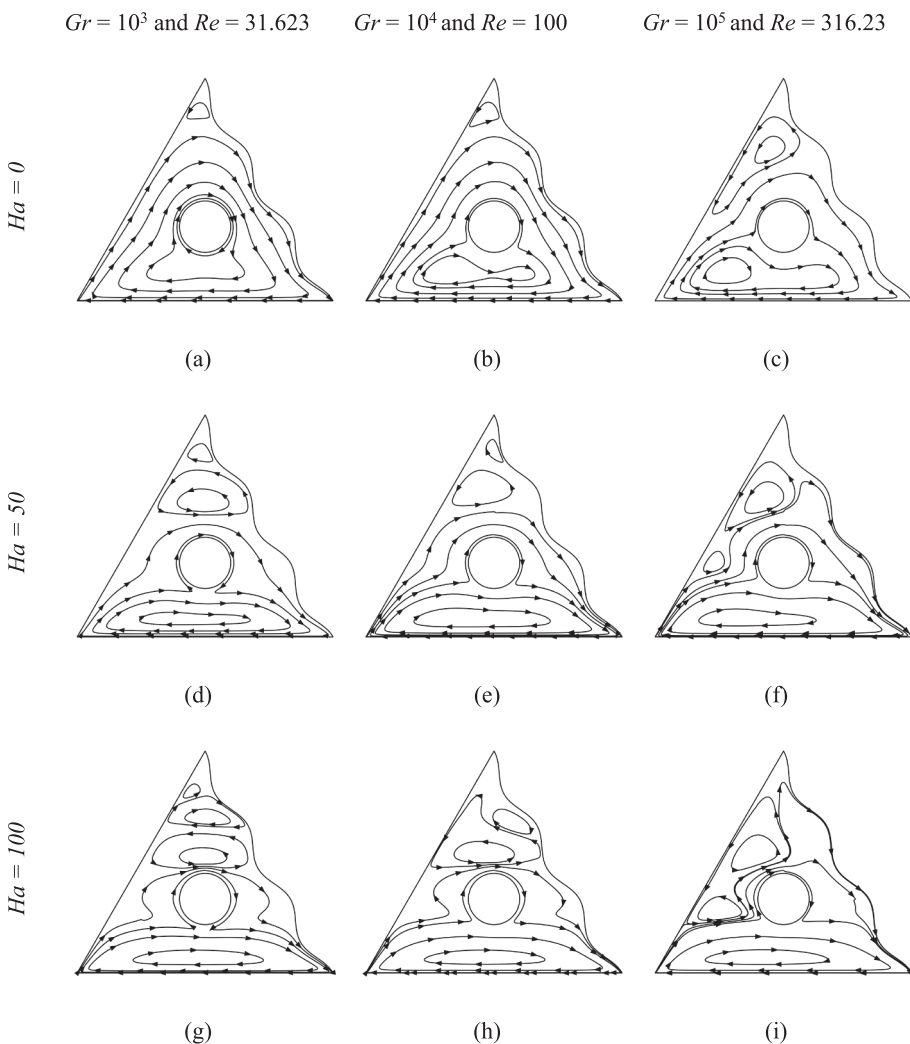


Fig. 16. Streamlines for various Re and Gr at (a)–(c) $Ha = 0$, (d)–(f) $Ha = 50$, (g)–(i) $Ha = 100$ when Ri is kept constant at 1.

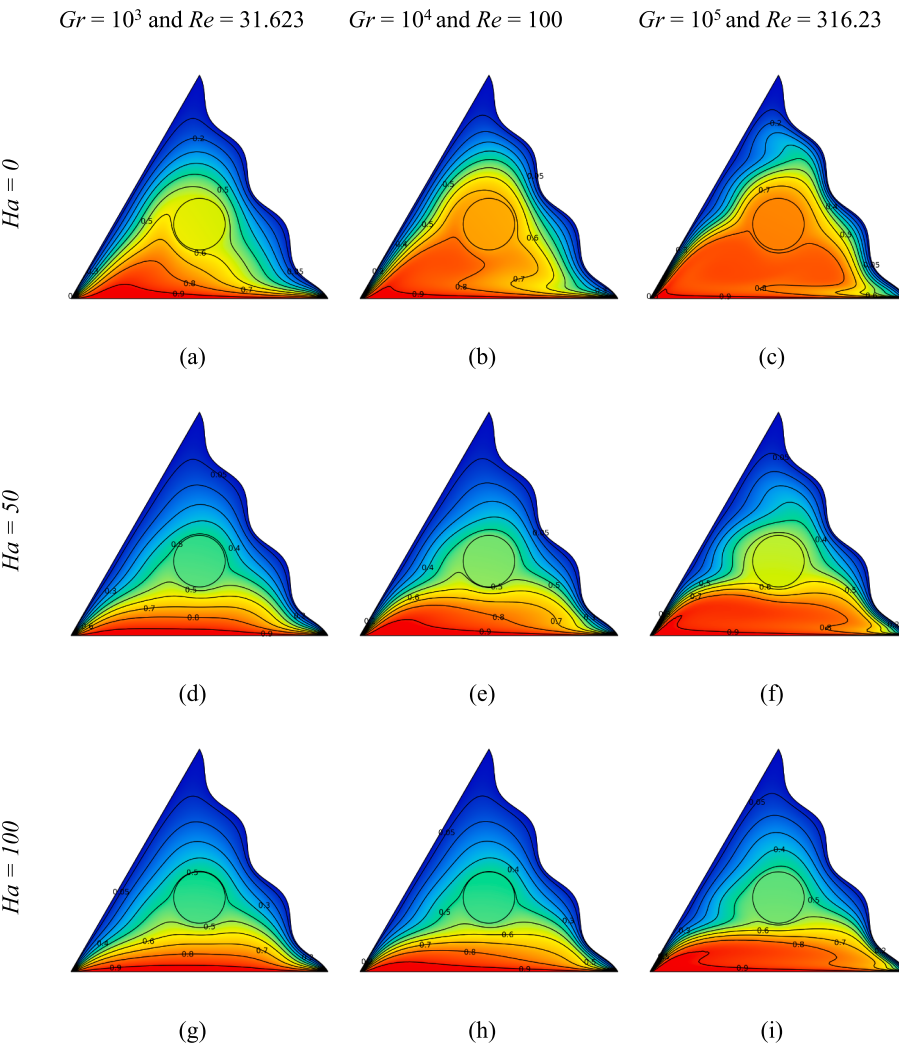


Fig. 17. Isotherms for various Re and Gr at (a)–(c) $Ha = 0$, (d)–(f) $Ha = 50$, (g)–(i) $Ha = 100$ when Ri is kept constant at 1.

6. Conclusion

This study conducted a comprehensive numerical investigation into mixed convection heat transfer within a lid-driven triangular wavy enclosure, focusing on the interplay between magnetic field intensity, internal heat generation, and a rotating heat-conductive cylinder. By varying key parameters, including the Hartmann, Reynolds, Grashof, and Richardson numbers, the study provides valuable insights into the thermal and fluid flow dynamics within geometrically complex enclosures. The principal findings of this investigation are as follows:

1. Enhanced Heat Transfer: The velocity of the moving bottom lid and the temperature gradient across the cold inclined wall and hot bottom wall significantly enhance heat transfer within the enclosure. Increased lid velocity and thermal gradients promote more effective convection, which is essential for optimizing thermal management systems.
2. Magnetic Field Modulation: The magnetic field intensity exerts a significant influence on the system's thermal performance, leading to a reduction in heat transfer as the Hartmann number increases. This reduction is primarily due to the suppression of convective currents by the Lorentz force, which diminishes fluid motion and creates a more uniform temperature distribution.
3. Impact of Wavy Walls and Vortices: The wavy walls within the enclosure introduce flow recirculation zones, which enhance heat

transfer. However, the effect of these walls becomes less pronounced at higher Hartmann numbers. Additionally, the formation of secondary vortices, particularly in natural convection scenarios, can reduce overall heat transfer by opposing the primary flow patterns.

4. Cylinder Rotation Effects: The direction and speed of the rotating cylinder within the enclosure critically affect vortex formation and thermal distribution. These effects are particularly pronounced when coupled with the influence of the magnetic field, leading to variations in heat transfer efficiency and fluid mixing.
5. Parametric Sensitivity and Optimization: The study reveals that the combined optimization of Reynolds, Grashof, and Hartmann numbers can be strategically utilized to fine-tune thermal performance. This sensitivity analysis highlights the importance of precise control over these parameters to achieve desired heat transfer outcomes in practical applications.
6. Heat Generation and Convection Regimes: The interaction between internal heat generation and the transition between forced and natural convection regimes is explored, showing that internal heat generation has a more pronounced impact in natural convection-dominated scenarios, leading to increased thermal stratification.

These findings contribute to a deeper understanding of the complex dynamics involved in mixed convection systems under the influence of magnetic fields and internal heat generation. The insights gained from this study have practical implications for optimizing thermal

management in various engineering applications, including chemical reactors, heat exchanger design, and solar energy systems. Future research should explore the effects of non-uniform magnetic fields, as the uniform field assumption is an idealization that may not fully represent real-world conditions. Additionally, investigating the use of liquid metals as working fluids could provide further insights into optimizing industrial applications. Furthermore, the impact of varying the cylinder's rotational speed on overall flow and thermal distribution should be examined to refine the understanding of system performance.

CRediT authorship contribution statement

Daud Hasan: Writing – review & editing, Writing – original draft, Visualization, Validation, Methodology, Formal analysis. **Arman Habib Polash:** Writing – review & editing, Writing – original draft, Visualization, Validation, Methodology, Formal analysis. **Hamim Faisal:** Writing – review & editing, Writing – original draft, Visualization, Validation, Methodology, Formal analysis. **Ahmed Intiaz Rais:** Writing – review & editing, Writing – original draft, Investigation, Formal analysis. **Md. Jisan Mahmud:** Writing – review & editing, Writing – original draft, Visualization, Validation, Supervision, Software, Methodology, Investigation, Formal analysis, Data curation, Conceptualization.

Declaration of competing interest

The authors declare that they have no known competing financial interests or personal relationships that could have appeared to influence the work reported in this paper.

Data availability

Data will be made available on request.

References

- Abu Bakar, N., Roslan, R., Md Akhir, M.K., 2020. The effects of internal heat generation or absorption on mixed convection in a lid-driven rectangular cavity using finite volume method. *CFD Lett.* 12 (12), 38–54. <https://doi.org/10.37934/cfdl.12.12.3854>.
- Ali, M.M., Akhter, R., Alim, M.A., 2022. Magneto-mixed convection in a lid driven partially heated cavity equipped with nanofluid and rotating flat plate. *Alex. Eng. J.* 61 (1), 257–278. <https://doi.org/10.1016/j.aej.2021.05.003>.
- Ali, M.Y., Alim, M.A., Karim, M.M., 2023. Mixed convective heat transfer analysis by heatlines on a lid-driven cavity having heated wavy wall containing tilted square obstacle. *Math. Probl. Eng.* 2023. <https://doi.org/10.1155/2023/1374926>.
- Al-Salem, K., Öztop, H.F., Pop, I., Varol, Y., 2012. Effects of moving lid direction on MHD mixed convection in a linearly heated cavity. *Int. J. Heat Mass Transf.* 55 (4), 1103–1112. <https://doi.org/10.1016/j.ijheatmasstransfer.2011.09.062>.
- Amine, B.M., Redouane, F., Mourad, L., Jamshed, W., Eid, M.R., Al-Kouz, W., 2021. Magnetohydrodynamics natural convection of a triangular cavity involving Ag-MgO/water hybrid nanofluid and provided with rotating circular barrier and a quarter circular porous medium at its right-angled corner. *Arab. J. Sci. Eng.* 46 (12), 12573–12597. <https://doi.org/10.1007/s13369-021-06015-6>.
- Azizul, F.M., Alsabery, A.I., Hashim, I., Roslan, R., Saleh, H., 2023. MHD mixed convection and heatlines approach of nanofluids in rectangular wavy enclosures with multiple solid fins. *Sci. Rep.* 13 (1). <https://doi.org/10.1038/s41598-023-36297-9>.
- Chamkha, A.J., 2002. Hydromagnetic combined convection flow in a vertical lid-driven cavity with internal heat generation or absorption. *Numer. Heat Transfer A Appl.* 41 (5), 529–546. <https://doi.org/10.1080/104077802753570356>.
- Chamkha, A.J., Selimefendigil, F., Öztop, H.F., 2018. MHD mixed convection and entropy generation in a lid-driven triangular cavity for various electrical conductivity models. *Entropy* 20 (12). <https://doi.org/10.3390/e20120903>.
- Chatterjee, D., Mondal, B., Halder, P., 2014. Hydromagnetic mixed convective transport in a vertical lid-driven cavity including a heat conducting rotating circular cylinder. *Numer. Heat Transfer A Appl.* 65 (1), 48–65. <https://doi.org/10.1080/10407782.2013.812399>.
- Cherif, B.M., et al., 2022. Hydrothermal and entropy investigation of nanofluid mixed convection in triangular cavity with wavy boundary heated from below and rotating cylinders. *Nanomaterials* 12 (9). <https://doi.org/10.3390/nano12091469>.
- Chowdhury, E.H., Al Mehedi, A., Paul, D.K., Saha, S., Ali, M., 2021. Conjugate pure mixed convection in a differentially heated lid-driven square cavity with two rotating cylinders. In: AIP Conference Proceedings. American Institute of Physics Inc. <https://doi.org/10.1063/5.0037523>
- Chowdhury, K., Alim, M.A., 2023. Mixed convection in a double lid-driven wavy shaped cavity filled with nanofluid subject to magnetic field and internal heat source. *J. Appl. Math.* 2023. <https://doi.org/10.1155/2023/7117186>.
- Hasan, N., Saha, S., 2024. Effects of internal heat production and Joule heating on MHD conjugate mixed convection and entropy production inside a thermally non-homogeneous cooling system. *Ann. Nucl. Energy* 206, 110671. <https://doi.org/10.1016/J.ANUCENE.2024.110671>.
- Hussain, Z., Alghamdi, M., Fozia, Ali, S., Ali, M.R., Aslam, M., 2023. Significance of mixed convective heat transfer model in an equilateral triangular enclosure subjected to cylindrical heated objects inside. *Case Stud. Therm. Eng.* 47. <https://doi.org/10.1016/j.csite.2023.103027>.
- Hussain, Z., Alghamdi, M., Muhammad, T., Anwar, M.S., 2024. Lid-driven effect on convective heat transfer with heated rods in a modified equilateral triangular cavity. *Case Stud. Therm. Eng.* 61, 104908. <https://doi.org/10.1016/j.csite.2024.104908>.
- Imtiaz Rais, A., Jisan Mahmud, M., Rakib Hossain, M., Saha, S., 2023. Influence of heat generation/absorption on mixed convective flow in a lid-driven chamber with isothermal rotating cylinder. *Ann. Nucl. Energy* 182. [https://doi.org/10.1016/j.anocene.2022.109596](https://doi.org/10.1016/j.anucene.2022.109596).
- Islam, A.N.M.F., Islam, R., Javed, S., Saha, S., 2024. Optimization of system parameters during conjugate mixed convective flow in a square domain with an oscillating spinning cylinder. *Heliyon* 10 (2). <https://doi.org/10.1016/j.heliyon.2024.e24258>.
- Jamy, R.H., Chowdhury, S., Chowdhury, F.K., Saha, S., 2023. Analyzing overall thermal behaviour of conjugate MHD free convection in L-shaped chamber with a thick fin. *Case Stud. Therm. Eng.* 48. <https://doi.org/10.1016/j.csite.2023.103137>.
- Mahmoudi, A., Mejri, I., Abbassi, M.A., Omri, A., 2014. Analysis of the entropy generation in a nanofluid-filled cavity in the presence of magnetic field and uniform heat generation/absorption. *J. Mol. Liq.* 198, 63–77. <https://doi.org/10.1016/j.molliq.2014.07.010>.
- Mahmud, M.J., Rais, A.I., Hossain, M.R., Saha, S., 2022. Conjugate mixed convection heat transfer with internal heat generation in a lid-driven enclosure with spinning solid cylinder. *Heliyon* 8 (12). <https://doi.org/10.1016/j.heliyon.2022.e11968>.
- Nishimura, T., Ohori, Y., Kawamura, Y., 1984. Flow characteristics in a channel with symmetric wavy wall for steady flow. *J. Chem. Eng. Jpn.* 17 (5), 466–471. <https://doi.org/10.1252/jcet.17.466>.
- Oztop, H.F., Al-Salem, K., Pop, I., 2011. MHD mixed convection in a lid-driven cavity with corner heater. *Int. J. Heat Mass Transf.* 54 (15–16), 3494–3504. <https://doi.org/10.1016/j.ijheatmasstransfer.2011.03.036>.
- Paul, D.K., Mehedi, A.A., Chowdhury, E.H., Saha, S., Ali, M., Amin, M.R., 2020. Conjugate mixed convection in a differentially heated lid-driven square cavity with rotating cylinders. doi: <https://doi.org/10.1115/IMECE2020-23339>.
- Rahman, M.M., Alim, M.A., Sarker, M.M.A., 2010. Numerical study on the conjugate effect of joule heating and magneto-hydrodynamics mixed convection in an obstructed lid-driven square cavity. *Int. Commun. Heat Mass Transfer* 37 (5), 524–534. <https://doi.org/10.1016/j.icheatmasstransfer.2009.12.012>.
- Rahman, M.M., Mojumder, S., Saha, S., Joarder, A.H., Saidur, R., Naim, A.G., 2015. Numerical and statistical analysis on unsteady magnetohydrodynamic convection in a semi-circular enclosure filled with ferrofluid. *Int. J. Heat Mass Transf.* 89, 1316–1330. <https://doi.org/10.1016/j.ijheatmasstransfer.2015.06.021>.
- Rasel, M.S., Rupam, M.T.I., Shuvo, M.S., Saha, S., 2023. Investigation on conjugate mixed convection through a vented chamber with heat generating and conducting rotating circular cylinders. *Results Eng.* 19. <https://doi.org/10.1016/j.rineng.2023.101248>.
- Ray, S., Chatterjee, D., 2014. MHD mixed convection in a lid-driven cavity including heat conducting circular solid object and corner heaters with Joule heating. *Int. Commun. Heat Mass Transfer* 57, 200–207. <https://doi.org/10.1016/j.icheatmasstransfer.2014.07.029>.
- Saha, L.K., 2015. Effect of internal heat generation or absorption on MHD mixed convection flow in a lid driven cavity. *Am. J. Appl. Math.* 3 (1), 20. <https://doi.org/10.11648/j.ajam.s.2015030101.13>.
- Selimefendigil, F., Öztop, H.F., 2016. Analysis of MHD mixed convection in a flexible walled and nanofluids filled lid-driven cavity with volumetric heat generation. *Int. J. Mech. Sci.* 118, 113–124. <https://doi.org/10.1016/j.ijmecsci.2016.09.011>.
- Selimefendigil, F., Öztop, H.F., Chamkha, A.J., 2016. MHD mixed convection and entropy generation of nanofluid filled lid driven cavity under the influence of inclined magnetic fields imposed to its upper and lower diagonal triangular domains. *J. Magn. Magn. Mater.* 406, 266–281. <https://doi.org/10.1016/j.jmmm.2016.01.039>.
- Selimefendigil, F., Öztop, H.F., Chamkha, A.J., 2017. Mixed convection in a partially heated triangular cavity filled with nanofluid having a partially flexible wall and internal heat generation. *J. Taiwan Inst. Chem. Eng.* 70, 168–178. <https://doi.org/10.1016/j.jtice.2016.10.038>.
- Selimefendigil, F., Öztop, H.F., Chamkha, A.J., 2019. Analysis of mixed convection and entropy generation of nanofluid filled triangular enclosure with a flexible sidewall under the influence of a rotating cylinder. *J. Therm. Anal. Calorim.* 135 (2), 911–923. <https://doi.org/10.1007/s10973-018-7317-5>.
- Shahid, H., Yaqoob, I., Khan, W.A., Rafique, A., 2021. Mixed convection in an isosceles right triangular lid driven cavity using multi relaxation time lattice Boltzmann method. *Int. Commun. Heat Mass Transfer* 128. <https://doi.org/10.1016/j.icheatmasstransfer.2021.105552>.
- Shekaramiz, M., Fathi, S., Ataabadi, H.A., Kazemi-Varnamkhasti, H., Toghraie, D., 2021. MHD nanofluid free convection inside the wavy triangular cavity considering periodic temperature boundary condition and velocity slip mechanisms. *Int. J. Therm. Sci.* 170. <https://doi.org/10.1016/j.ijthermalsci.2021.107179>.
- Sivasankaran, S., Sivakumar, V., Hussein, A.K., Prakash, P., 2014. Mixed convection in a lid-driven two-dimensional square cavity with corner heating and internal heat

- generation. Numer. Heat Transfer A Appl. 65 (3), 269–286. <https://doi.org/10.1080/10407782.2013.826017>.
- Sojoudi, A., 2018. Lattice Boltzmann simulation of mixed convection flow in a lid-driven triangular cavity subjected to sinusoidal thermal forcing utilizing nanofluid. Am. J. Fluid Dyn. 8 (3), 84–95. <https://doi.org/10.5923/j.ajfd.20180803.02>.
- Soomro, F.A., Haq, R.U., Algehyne, E.A., Tili, I., 2020. Thermal performance due to magnetohydrodynamics mixed convection flow in a triangular cavity with circular obstacle. J. Energy Storage 31. <https://doi.org/10.1016/j.est.2020.101702>.
- Tasnim, S., Shuvo, M.S., Deb, N., Islam, M.S., Saha, S., 2023. Entropy generation on magnetohydrodynamic conjugate free convection with Joule heating of heat-generating liquid and solid element inside a chamber. Case Stud. Therm. Eng. 52. <https://doi.org/10.1016/j.csite.2023.103711>.
- Uddin, M.N., Farhana, A., Alim, A., 2015. Finite element analysis of magneto-hydrodynamic (Mhd) mixed convection flow in a lid-driven triangular cavity. J. Nav. Archit. Mar. Eng. 12 (1), 21–32. <https://doi.org/10.3329/jname.v12i1.12910>.
- Younis, O., Ahmed, S.E., Abderrahmane, A., Alenazi, A., Hassan, A.M., 2023. Hydrothermal mixed convection in a split-lid-driven triangular cavity suspended by NEPCM. Mathematics 11 (6). <https://doi.org/10.3390/math11061323>.